Tikrit Journal of Engineering Sciences (2024); 31(3): 246-257
DOI: http://doi.org/10.25130/tjes.31.3.23

IRAQI Academic Scientific Journals

ISSN: 1813-162X (Print); 2312-7589 (Online)

Tikrit Journal of Engineering Sciences

available online at: http://www.tj-es.com

TJES Tikrit Journal of Engineering Sciences

Study the Thermal Performance of a PCM Layer-Filled Triple Glazed Window under Iraqi Climate Conditions

Mina A. Nsaif [a*], **Jalal M. Jalil** [b], **Mounir Baccar** [a]

[a] Advanced Fluid Dynamics, Energetics and Environment Laboratory, Department of Mechanical Engineering, National School of Engineers of Sfax, University of Sfax, Tunisia.

[b] Electromechanical Engineering Department, University of Technology, Baghdad, Iraq.

Keywords:

Triple-glazed window; PCM; CFD; Phase change materials; Thermal performance.

Highlights:

- *Design triple glazed window with PCM.*
- *The internal surface temperature of the TW-PCM was 3.1 °C lower than TW.*
- *TW-PCM increased thermal time lag by 2 hr.*

ARTICLE INFO

Article history:

Received	12 Jan.	2024
Received in revised form	28 Apr.	2024
Accepted	17 May	2024
Final Proofreading	27 Aug.	2024
Available online	15 Nov.	2024

© THIS IS AN OPEN ACCESS ARTICLE UNDER THE CC BY LICENSE. http://creativecommons.org/licenses/by/4.0/

Citation: Nsaif MA, Jalil JM, Baccar M. **Study the Thermal Performance of a PCM Layer-Filled Triple Glazed Window under Iraqi Climate Conditions**. *Tikrit Journal of Engineering Sciences* 2024; **31**(3): 246-257.
http://doi.org/10.25130/tjes.31.3.23

Corresponding author:

Mina A. Nsaif

Advanced Fluid Dynamics, Energetics and Environment Laboratory, Department of Mechanical Engineering, National School of Engineers of Sfax, University of Sfax, Tunisia.

Abstract: This paper evaluates the thermal performance of a simple triple-glazed window filled with a layer of paraffin wax (PCM) to reduce heat transfer through building openings. This research compared the performance of a traditional triple-glazed window with air gaps. The comparison was made using numerical modeling and experimental approaches. The experiment took a full day, and technical-grade paraffin was used as a PCM to fill a 20-mm gap between triple-glazing units. The temperature of the inner glass, the exterior surface, and both gaps of the glazed window were measured. The thermal performance of a triple-glazing window was evaluated numerically using a finite volume algorithm. The results showed that the solar radiation reached its maximum at 580 W/m² in March, and the internal surface temperatures of the normal triple-glazed window (TW) and integrated with PCM (TW-PCM) were 37.1 and 34 °C, respectively. The obtained temperatures of the TW-PCM decreased by 3.1°C compared to the TW. Furthermore, the TW-PCM demonstrated an increased time lag of 2 hours, effectively delaying the peak load.

دراسة الأداء الحراري لنافذة زجاجية ثلاثية مملوءة بطبقة PCM في ظل الظروف المناخية العراقية

مينا عبد الكريم نصيف[١]، جلال محمد جليل [٢]، منير بكار [١]

[١] مختبر ديناميكا الموائع والطاقة والبيئة المتقدمة / المدرسة الوطنية لمهندسي صفاقس / قسم الهندسة الميكانيكية / جامعة صفاقس / تونس.

[٢] قسم هندسة الكهروميكانيك / الجامعة التكنولوجية / بغداد – العراق.

الخلاصة

يقوم هذا البحث بتقييم الأداء الحراري لنافذة زجاجية ثلاثية بسيطة مملوءة بطبقة من شمع البارافين (PCM)، بهدف تقليل انتقال الحرارة من خلال فتحات المبنى. قام هذا البحث تحديدًا بمقارنة أداء النوافذ الزجاجية الثلاثية التقليدية ذات الفجوات الهوائية. تم إجراء المقارنة باستخدام كل من النمذجة العددية والأساليب التجريبية. استغرقت التجربة يومًا كاملاً، وتم استخدام البارافين التقني كـ PCM لملء فجوة بمقدار ٢٠ ملم بين وحدات الزجاج الثلاثي. تم قياس درجة حرارة الزجاج الداخلي والسطح الخارجي وفراغات النافذة الزجاجية. تم تقييم الأداء الحراري لنافذة ذات زجاج ثلاثي عدديا باستخدام خوارزمية الحجم المحدود. أظهرت نتائج البحث أنه في شهر مارس، عندما وصل الإشعاع الشمسي إلى حده الأقصى عند ٥٨٠ واط/م٢، كانت درجات حرارة السطح الداخلي للنافذة ذات الزجاج الثلاثي العادي (TW) ٣٧,١ درجة مئوية والمدمجة مع TW- PCM (PCM) ٣٤ درجة مئوية. على التوالي. انخفضت درجات الحرارة التي تم الحصول عليها لـ TW-PCM بمقدار ٣,١ درجة مئوية مقارنة بـTW. علاوة على ذلك، أظهر TW-PCM فارقًا زمنيًا متزايدًا قدره ساعتين، مما أدى إلى تأخير الحمل الأقصى بشكل فعال.

الكلمات الدالة: نافذة زجاجية ثلاثية، PCM، CFD، مواد متغيرة الطور، الاداء الحراري.

1.INTRODUCTION

The growing population and technological developments have driven global energy sector demand [1-2]. Buildings accounted for 20.1% of global energy used in 2016 [3]. Outdoor solar radiation affects the buildings' energy consumption. Therefore, the building envelope is one of the most important energy-saving factors. Effective energy-saving or interior thermal comfort strategies involve latent heat thermal energy storage systems using Phase Change Materials (PCMs) in the building envelope [4–7]. Xie et al. [8] found that PCM-based building envelopes can reduce indoor heating and cooling loads due to fluctuating external conditions and balancing heat energy supply and demand. Due to PCMs' temperature, PCM-based envelopes for buildings can also reach 22–28 °C, which is within human comfort [9]. Energy-saving glazing modules have been the subject of numerous studies and projects over the past few decades. Among these, one of the most significant solutions for reducing buildings cooling or heating loads is using (PCM) in windows. The importance of window treatments as a green building technology is particularly pronounced in countries with significant seasonal climate changes, such as Iraq. Certain PCMs are an excellent option for filling glazing windows because they have low infrared, ultraviolet, and high visible light transmittance, allowing them to minimize solar heat entering indoor spaces without compromising illumination. Several researchers have been very interested in this topic since it may simultaneously lower energy usage of buildings and increase interior thermal comfort. Abbas et al. [10] examined a numerical and experimental study incorporating phase change material (PCM) capsules as insulation within hollow bricks constituting a building. The findings indicated that encapsulating Phase Change Materials (PCM) in the treated wall could drop room temperatures and the wall's inner surface temperatures. Jalil et al. [11] used heat sinks to cool electronic equipment with phase change material. The examination used numerical simulations and experiments. The study considered varied input power levels (11, 13, and 15) W and airflow velocities of (3.4, 2.5, and 1.5) m/s. The authors conducted two case studies: with and without PCM. Investigating PCM thickness and nanomaterial incorporation. The experiment revealed that using a heat sink combined with PCM resulted in a temperature reduction of 18 °C. This paper investigated the impact of incorporating nanoparticles (Al_2O_3) into PCM, and a small quantity of nanoparticles (2%) enhanced the efficiency of the heat sink. Wieprzkowicz and Heim [12] numerically analyzed a complex triple-glazed (PCM) window. Windows' advanced control algorithm changes phase-changed optical characteristics and explains the control/actuator algorithm and its integration into ESP-r. Cooling and lighting energy usage, visual irritation, glare, and thermal discomfort were assessed. The investigation found that partitioning the glazing into areas filled with PCM with different melting temperatures is the best way to use PCM. For thermal impact, Dheyab et al. [13] studied an absorber-finned heat exchanger-thermal storage unit in a solar air heater. The experiments were conducted in December 2021 and January 2022 in Tikrit, Iraq, using two solar air (SAH) using RT42 and RT50 PCMs. Each PCM filled the SAH thermal storage. A finned heat exchanger drove the air in the thermal storage. Two setups were tested. The first configuration included separated SAHs. The second setup combined the RT42 and RT50 SAHs in series. In the separation configuration, RT50 reached 59 °C, i.e., the highest temperature. Ahmed et al. [14] conducted a comprehensive review of the literature on PV-Trombe wall system designs, detailing how design and operational parameters, such as direct current fan use, facade width air vent, air gap thickness, thermal insulation, packing factor, heat storage, air mass flow rate, PV cell cooling, southern windows, and solar cell tilt angle, affect PV-Trombe wall performance. Additionally, the PV-Trombe wall system was compared to the standard Trombe wall, and its applicability was discussed. Engineers and researchers might use this review article for future studies. Ahmed et al. [15] constructed, validated, and employed 1D equations of steady-state energy balance for the bi-fluid configuration to forecast the system's performance for various air and water mass flow rates. For average daily evaluation, bi-fluid with DC fan-glazed and unglazed PV-TW systems had 79.89% and 10.69% thermal and electrical efficiencies, respectively, under 300 liters/day. The highest difference between theoretical and experimental solar cell temperature data was less than 4%. Abbas and Azat [16] investigated the impact of mass flow rate and Rayleigh number on passive Trombe walls using industrial wax as a PCM. A PVC sandwich panel test setup was built without the south wall. Trombe walls received a 6 mm transparent glass coating. The six winter studies in Kirkuk City used six air gap channel widths. These widths were 10–35 cm. Experimental results revealed that mass flow rate was directly related to channel width and inversely to Rayleigh number. The efficiency was 2.45 times higher at 30 cm than at 10 cm. Salih et al. [17] investigated the thermal performance of a double-pass solar air heater using PCM-based rectangular capsules filled with paraffin wax. The results indicated that high airflow rates delayed the paraffin melting. Zhang et al. [18] examined SSPCMs' thermal-optical performance in glazing windows. The ideal melting temperature, latent heat, absorption index, and refractive index for SSPCM in specified property ranges were 18 °C, 120 kJ/kg, 60 m^{-1}, and 1.3, respectively. Kułakowski [19] investigated the best solution for triple-glazed windows with one cavity filled with PCM. The simulation recommended a solution for PCM thicknesses, locations, and temperatures. The computational model was developed, tested, and verified numerically. The ideal solution was found using the fuzzy sets approaches. Both approaches indicated a version with a PCM layer in the inner chamber and an average melting temperature of 25 °C. However, fuzzy sets established ideal PCM thicknesses ranging from 5 to 20 mm using multiple criteria and linguistic characteristics. Wang et al. [20] used numerical simulation to study the rupture behavior and thermal-structural connection of a paraffin wax-containing glass envelope under fire conditions. The double-glazing unit filled with paraffin wax exhibited enhanced fire resistance compared to a standard unit. Li et al. [21] examined an innovative roof based on SA-PCM glazing systems, and a numerical model was built to explain how PCM fill ratio and cavity arrangement models affect photothermal and energy performance. PCM improved the thermal performance of the novel roof, reducing the magnitude and increasing the phase shift of temperature waves on the inner surface. Recently, Li et al. [22] examined how PCM thermophysical factors affect the double-glazing unit thermal performance. As PCM density, thermal conductivity, specific heat capacity, latent heat, and melting temperature increased, the temperature time lag of the PCM-filled double-glazing unit increased, and the temperature decrement factor decreased. Increasing PCM density, latent heat, and melting temperature improved the thermal performance in double-glazed units. However, increasing the thermal conductivity and specific heat capacity beyond 2.1 W/ (m.K) and < 4460 J/ (kg K) was ineffective. The studies above demonstrated that PCM-filled glazing windows can be implemented in buildings to increase energy efficiency and improve thermal comfort. Nevertheless, as further study was conducted, new issues about PCM-filled glazing units emerged, including the occurrence of overheating after the PCM entirely melted and releasing latent heat during summer nights [23]. Li et al. [24] found that the first type had a poor thermal performance on a typical summer night because the solar energy would be released by the PCM, which absorbed it during the day, rendering it ineffective in its ability to reduce energy usage and improve the thermal comfort of interior spaces. These studies showed that there must be further research on improvements to the PCM-filled glazing windows, as current investigations still require fully addressing these issues. Jalil and Salih [25] looked at how changing the thermal properties of paraffin wax affected the performance of a double-glazed window doped with paraffin wax in Baghdad during the summer. The results showed that increasing the temperature-time lag (TTL) and decreasing the double-glazed window's temperature decrement factor (TDF) improved the unit work because the PCM's density, latent heat, and thickness improved. Jalil and Salih [26] computationally and experimentally evaluated the PCM effectiveness in double-glazed windows in improving the comfort of a room and thermal performance in Iraq. In the present study, standard glass windows had low insulation, and the outer temperature surface significantly increased. Therefore, PCM will be applied to absorb the heat and improve window insulation. A new arrangement of triple-glazing windows filled with phase-change material has been suggested. Addressing existing restrictions, this new design seeks to maximize energy savings and indoor thermal comfort by improving the thermal transfer characteristics of glass windows. The present study experimentally and numerically investigated two triple-glazed windows filled with PCM as an insulating material to improve their thermal performance in the Iraqi environment in March. Two windows were built as follows:

1) TW-Normal: This is a triple-glazed window with air in the outer and inner gaps.
2) TW-PCM: In this configuration, the outer gap contained PCM with a melting point of 44°C, and the inner gap contained air.

Temperature readings were meticulously recorded from each cavity and the internal and external surfaces of both windows to assess the insulative capabilities of all the triple-glazed windows throughout the day under varying conditions of solar incidence. The insulative performance assessment depended on the windows' self-regulated internal surface temperatures.

2.EXPERIMENTAL WORK

This section explains the proposed design of the window, the operational principle, the experimental setup, the PCM properties, and the instrumentation. Figure 1 depicts the system: a three-layer glass window with two gaps separating it and a layer of paraffin acting as an insulating material to reduce thermal conduction. To minimize heat transfer, spacers secure the windows to the frame and space them apart. The experiment used two types of triple-glazed windows. In the first window, the gaps were maintained with air (TW-Normal), and in the second window, the external gap of the triple-glazed window (TW-PCM) was filled with phase change materials (PCM) having a melting point of 44 °C (2.5 kg), and the other gap contained air. The cost of one kilogram of PCM was $11. The dimensions of the test room were 1.5 × 1.5 × 1.5 m. These two types of windows had a length of 41 cm, a width of 41 cm, a gap of 2 cm, and a glass thickness of 6 mm. The experiment used halogen lamps to simulate solar radiation. Table 1 displays the thermophysical properties of PCM. The schematic structure of two triple-glazed windows is shown in Fig.2. The heat transfer triple-glazing system combined the exterior glass, the cavity layer, and the interior glass. Table 2 shows the temperature measurements used in the test, and Table 3 shows the physical properties of the glass used. Figure 3 depicts the melting and frosting cycles of the Phase Change Material (PCM) throughout the day. The quantity of solar radiation the (TW-PCM) system received determines this process. Fundamentally, the higher the solar radiation incident, the earlier and more rapidly the PCM begins to melt.

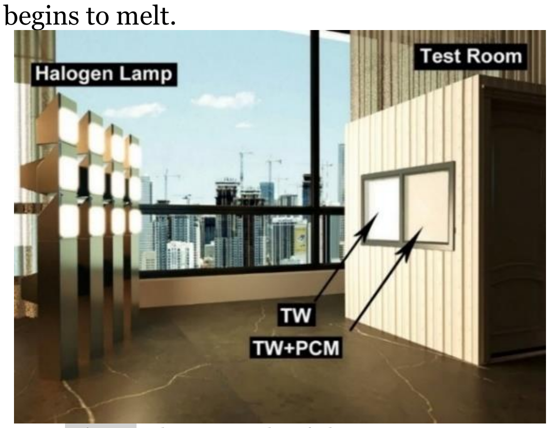

Fig. 1 Photograph of the Test Room.

Table 1 Thermo-Physical Properties of Phase Change Material (PCM) [27].

Material	Melting Temp. (°C)	Specific heat (kJ kg⁻¹ K⁻¹)		Density (kg. m⁻³)		Latent Heat of Fusion (J kg⁻¹)	Thermal Conductivity (W m⁻¹ K⁻¹)
		Solid	Liquid	Solid	Liquid		
PCM	44	2.1	2.1	930	830	190	0.21

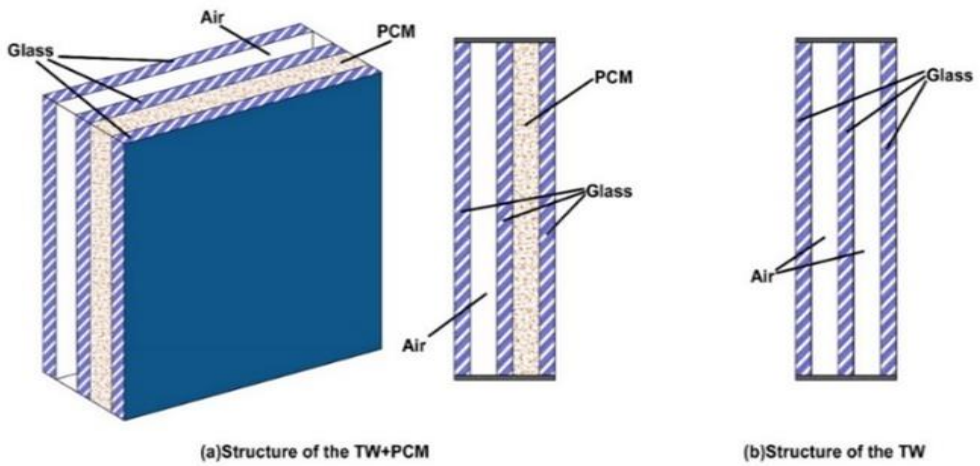

Fig. 2 Schematic Structure of a Triple Glazed Window with and without PCM Layer.

Table 2 Displays the Temperature Measuring Device.

Instrument	Explain
Thermocouples	Eight thermocouples (type K) were utilized to determine the temperature distribution across the room. Two stainless steel wires were installed inside the room in an X configuration, extending lengthwise from the north side to the south side.
Thermometer Device	The HT-9815 model thermometer was utilized to record the temperature. This device has four channels. The probes of the thermocouples, which were distributed in the room, inside and outside surfaces of the triple-glazed window, in each gap for four windows, were connected to these channels. The data will be recorded manually.
Solar Power Meter	A digital (SM206-SOLAR) radiation meter was used to measure incident radiation from Halogen lamps in the surface area of four TW. The instrument has a response time of 1 second and measures the radiation intensity in the range of 0.1 to 1999 W/m2.

Table 3 Displays the Physical Properties of Glass [28].

	Glazing			
	Emissivity	Solar transmittance at typical incidence	Solar reflectance at normal incidence	Thickness (m)
Clear Glass	0.84	0.804	0.074	0.006

11:00 AM 12:00 PM 1:00 PM 2:00 PM

(a)

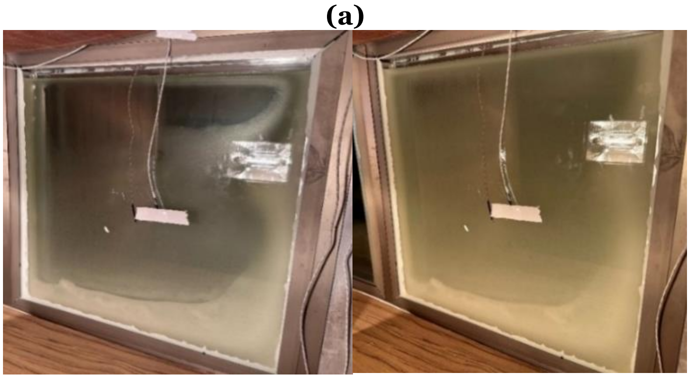

03:00 PM 04:00 PM

(b)

Fig. 3 Process of the PCM in March Month of (TW – PCM) in Various Time: A) Melting, B) Re-Solidification.

2.1.Experimental Procedure (Steps)

The solar radiant heat directed at each triple-glazed window remained consistent. The power source remained stable with no voltage fluctuations, which is crucial since it influenced the concentration of the halogen lamps. The testing period lasted from 6 AM to 9 PM. The following producer was taken:

1) Verify that all thermocouple investigations are linked to the thermometer.
2) link the dimmer to the halogen lamps.
3) The cooler device is functioning properly.

Table 4 lists the reliability of the devices used to estimate temperature and radiation.

Table 4 Measuring Device Accuracy**.**

Parameter	Instrument	Model	Range	Accuracy
Temperature	Thermometer	HT-9815	–100 to 1300 °C	± 0.15%
	Thermocouple	Type-K	–100 to 1300 °C	± 0.4%
Solar radiant heat	Solar power meter	SM206-SOLAR	0.1 to 1999 W/m²	± 5%

2.2. Uncertainty Analysis

To make the results more accurate, the uncertainty in the triple-glazed windows can be estimated using the error rate detected in the instruments used in practical experiments [29]. Then, the uncertainty of heat will be;

$$\delta Q/Q = [(\delta T/T)^2]^{1/2} \quad (1)$$

3. NUMERICAL FORMULATIONS

Partial Differential Equations (PDEs) are extensively used to analyze and predict the thermic attitude of various systems. In the domain of building physics and architecture, window systems are essential. The test chamber, featuring two types of triple windows with dual cavities, offered an excellent heat barrier compared to standard triple-glazed alternatives. The triple-glazed window system minimized energy loss from its bottom and side windows by employing efficient insulation. The numerical solution performed under the following underlying assumptions:

1) Three dimensions and all analyses were transient.
2) Constant air properties.
3) The effects of energy dispersion, buoyancy, and body force were ignored.
4) All properties were assessed at the mean temperature.

3.1. Thermal Analysis Model

Figure 5 presents the analysis of the TW windows using a 3-dimensional transient model. Detailing the thermal system simulation is crucial for predicting various factors that might affect the thermal performance of window under different environmental conditions. The model simplifies understanding of heat transfer processes, i.e., conduction and convection, within the multi-layered structure of the TW. In the case of conduction, $a = \frac{kg*dt}{dg*dx^2}$, and in the case of convection, $a = \frac{h*dt}{dg*dx}$. The model employs the concept of small, six-faced elements, i.e., representing the north, south, east, west, low, and high sides, within a control volume to establish an energy equilibrium. This approach suggests that the collection of heat entering and departing the window configuration is balanced, achieving a pure zero.

$$\sum q_{\text{in all face}} - \sum q_{\text{out all face}} = q_{\text{storage}} \quad (2)$$

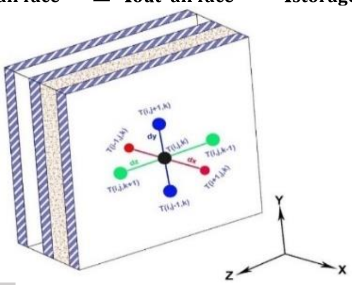

Fig. 5 3-Dimension Nodes for Suggested Triple Glazed Window.

Triple Glazed Window (PCM – Air)

For Glass

Energy Equation

In this system will be used energy of equation to calculate the enthalpy at each node across three dimensions.

At x=0, experimental surface temperature.

At x=l_x, convection heat transfer.

At y=0, y= l_y, z=0, and z=l_z , insulate.

Initial condition, ambient temperature

For the central node, all boundary conditions are under conduction mode.

$$a_e = a_w = \frac{kg*dt}{dg*dx^2} \quad (3)$$

$$a_s = a_n = \frac{kg*dt}{dg*dy^2} \quad (4)$$

$$a_t = a_b = \frac{kg*dt}{dg*dz^2} \quad (5)$$

$$enew_{(i,j,k)} = a_e T_{(i+1,j,k)} + a_w T_{(i-1,j,k)} + a_n T_{(i,j+1,k)} + a_s T_{(i,j-1,k)} + a_t T_{(i,j,k+1)} + a_b T_{(i,j,k-1)} - (a_n + a_s + a_e + a_w + a_t + a_b) * T_{(i,j,k)} + eold_{(i,j,k)} \quad (6)$$

3.2. With PCM Model

The physical type of this PCM was assumed to be homogeneous and anisotropic. This assumption was fundamental in selecting a transient scheme for the modeling. The enthalpy transformation method was employed to incorporate the enthalpy into the energy equation of the PCM, serving as the foundation for its mathematical representation. The convective term and viscous dissipation were considered negligible in this particular model. Cao [30] developed the following 3-dimensional energy equation model based on these premises:

$$\frac{\partial}{\partial x}\left(k\frac{\partial T}{\partial x}\right) + \frac{\partial}{\partial y}\left(k\frac{\partial T}{\partial y}\right) + \frac{\partial}{\partial z}\left(k\frac{\partial T}{\partial z}\right) = \rho\frac{\partial H}{\partial t} \quad (7)$$

The state equation is,

$$\frac{\partial H}{\partial T} = C_p \quad (8)$$

All phases are characterized by having an equal heat capacity, and the phase transition occurs at a constant temperature [31,32].

$$T = \begin{cases} T_{melt} + {}^{H}/_{C_{ps}} & H \le 0 \quad (solid\ phase) \\ T_{melt} & 0 < H < L \quad (phase\ change) \\ T_{melt} + (H - L)/C_{pl} & H \ge L \quad (liquid\ phase) \end{cases} \quad (9)$$

For the condition H=0, the phase change material (PCM) is in its solid state. The Kirchhoff temperature transformation was employed [33].

$$T^* = \int_{T_m}^{T} k(\eta)d\eta = \begin{cases} k_s(T - T_{melt}), & T < T_{melt} \\ 0, & T = T_{melt} \\ k_l(T - T_{melt}), & T > T_{melt} \end{cases} \quad (10)$$

The subsequent equation was derived by transforming Eq. (8) and integrating the expression from Eq. (9).

$$T^* = \begin{cases} k_s H / C_{ps}, & H \le 0 \\ 0, & 0 < H < L \\ k_l (H - L) / C_{pl}, & H \ge L \end{cases} \quad (11)$$

So, the function of enthalpy was displayed as,

$$T^* = \lambda(H)H + S(H) \quad (12)$$

The specific temperature at which the phase change occurs is determined as follows:

$$\lambda(H) = \begin{cases} k_s/C_{ps}, & H \le 0 \\ 0, & 0 < H < L \\ k_l/C_{pl}, & H \ge L \end{cases} \quad (13)$$

In addition,

$$S(H) = \begin{cases} 0, & H \le 0 \\ 0, & 0 < H < L \\ -\frac{Lk_l}{C_{pl}}, & H \ge L \end{cases} \quad (14)$$

Substituting Eq. (11) in Eq. (6) gives:

$$\rho \frac{\partial H}{\partial t} = \frac{\partial}{\partial x}\left(\frac{\partial(\lambda H)}{\partial x}\right) + \frac{\partial}{\partial y}\left(\frac{\partial(\lambda H)}{\partial y}\right) + \frac{\partial}{\partial z}\left(\frac{\partial(\lambda H)}{\partial z}\right) + p \quad (15)$$

With the term,

$$p = \frac{\partial}{\partial x}\left(\frac{\partial S}{\partial x}\right) + \frac{\partial}{\partial y}\left(\frac{\partial S}{\partial y}\right) + \frac{\partial}{\partial z}\left(\frac{\partial S}{\partial z}\right) \quad (16)$$

Equation (6) can be formulated as follows for the solid region:

$$\rho \frac{\partial H}{\partial t} = \frac{\partial}{\partial x}\left(k_s \frac{\partial T}{\partial x}\right) + \frac{\partial}{\partial y}\left(k_s \frac{\partial T}{\partial y}\right) + \frac{\partial}{\partial z}\left(k_s \frac{\partial T}{\partial z}\right) \quad (17)$$

Also, in the liquid region.

$$\rho \frac{\partial H}{\partial t} = \frac{\partial}{\partial x}\left(k_l \frac{\partial T}{\partial x}\right) + \frac{\partial}{\partial y}\left(k_l \frac{\partial T}{\partial y}\right) + \frac{\partial}{\partial z}\left(k_l \frac{\partial T}{\partial z}\right) \quad (18)$$

When Eq. (6) is modified to exclude the convection term and is applied specifically within the phase change region, it produces the following expression:

$$\rho \frac{\partial H}{\partial t} = \frac{\partial^2}{\partial x^2}(\lambda H) + \frac{\partial s^2}{\partial x^2} + \frac{\partial^2}{\partial y^2}(\lambda H) + \frac{\partial s^2}{\partial y^2} + \frac{\partial^2}{\partial z^2}(\lambda H) + \frac{\partial s^2}{\partial z^2} \quad (19)$$

where for $S = S(H)$ and $\lambda = \lambda H$, the above equations can be reformulated using the finite-volume method with an explicit scheme as:

$$\iiint_V \rho \frac{\partial H}{\partial t} = \rho \Delta V \left(\frac{H_p - H_p^o}{\Delta t}\right) \quad (20)$$

In this context, H_p^o is represented as the previous value of H at grid point P. In the final setup, the mesh size for each window was set at (59, 11, 11) in the (x, y, z) dimensions. Using an explicit scheme, the simulation employed a finite volume method with transient equations. The time step for this process was set at 0.05 seconds.

3.3. Validation of the Numerical Results

Figure 6 (a) and (b) compares the numerical and experimental results regarding temperature variations on the internal surfaces of two types of triple-glazed windows. The correlation between these numerical and experimental outcomes was considered satisfactory.

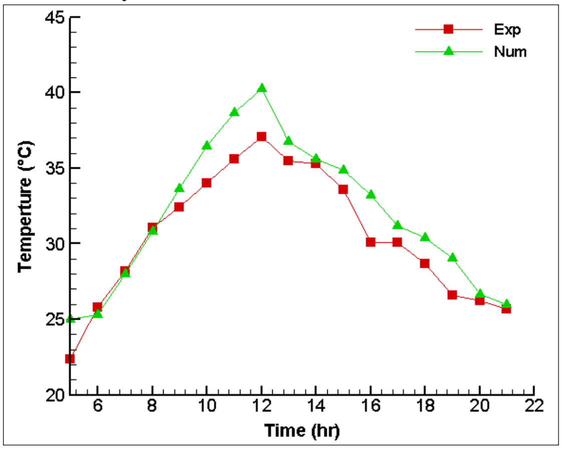

(a)

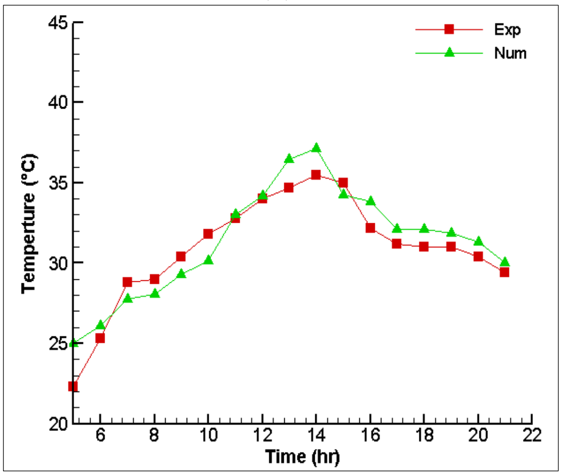

(b)

Fig. 6 Validation of Numerical Results with Experimental Results of Internal Surface Temperature of The Window in March (a) TW, (b) TW- PCM.

4. FINDINGS AND DISCUSSION

The current study evaluated a model both numerically and experimentally using the FORTRAN programming language. The objective was to estimate the effect of integrating PCM as insulation materials into the cavities of TW. The experimental measurements were conducted over a one-month period, specifically in March 2023, under consistent conditions. To ensure the accuracy of the results, these experimental tests were repeated on multiple days. During the trials, radiance levels and various temperature readings were recorded every 60 minutes. The most significant temperature fluctuations were observed on a particular day, showcasing the effectiveness of thermal storage. This effectiveness was primarily due to the PCM's ability to solidify at low night temperatures and melt during the day, aided by high ambient temperatures and solar radiation. The observed temperature variation between day and night underscored the potential of PCM to improve thermal performance in such applications. One of the insulation technologies is integrating PCM into building envelopes, which adds thermal mass to walls without requiring large value of material. A small amount of PCM can realize significant heat during the phase change. When embedded in the building envelope, PCM absorbs and stores heat from the outside during the day and releases it when the temperature drops below its melting point. This process helps lower inner air temperature, shift peak loads, and lower indoor temperature variation.

4.1.Experimental and Numerical Temperature Results

Figure 7 depicts the solar radiation patterns and air temperature inside the test room observed during the experimental days. The highest southern solar radiation was recorded in March at 12 PM. Figure 8 depicts the inside temperature of the two studied windows with glazing. The maximum glass temperature at high solar 580 W/m^2 at 12 PM was 37.1 °C for windows without PCM (TW), whereas it was only 34 °C in windows with PCM (TW-PCM). Additionally, through the daytime, from 6 AM to 1 PM, the temperature in TW was higher than TW-PCM and lower during the nighttime from 3 PM to 9 PM due to the wax's phase change between solid and liquid. Overall, the temperature difference (external and internal) was low in TW-PCM. Therefore, using PCM in glass windows reduced by approximately 3.1°C. Figure 9 shows the external temperature comparison. The temperatures from 6:00 AM to 2:00 PM were similar in both windows. However, from 3 PM to 9 PM, the temperatures of TW-PCM were higher due to wax melting and releasing the storage heat. Figure 10 (a) and (b) displays the temperatures in the outer and inner gaps of windows. The temperatures in the inside and outside gaps of TW-PCM were lower than TW between 6 AM and 2 PM due to the PCM's ability to absorb and store heat. After 2 PM, the temperatures in TW's outer and inner gaps were lower than TW-PCM due to the PCM completely melting and transferring the stored heat to the internal gap, subsequently radiating it to the inner surface. Figure 11 (a, b, c, and d) shows the three – dimension of the isothermal contours for TW-PCM at 9 AM, 11 PM, 12 PM, and 4 PM, respectively. The internal surface temperature was 30.4, 32.8, 34, and 32.2 °C at 9 AM, 11 PM, 12 PM, and 4 PM, respectively. In addition, Figure 11 shows that areas highlighted in green represent lower temperatures, which are the optimal conditions for PCM to function effectively. The red region indicates high temperatures, suggesting areas that receive greater solar radiation levels. The sections close to the melting point of the PCM (44°C), demonstrating active heat absorption, indicate the PCM's effectiveness. The overall of the PCM insulation technologies was evaluating success that would be based on the amount of green and yellow patches, representing low temperatures and hence implying better performance.

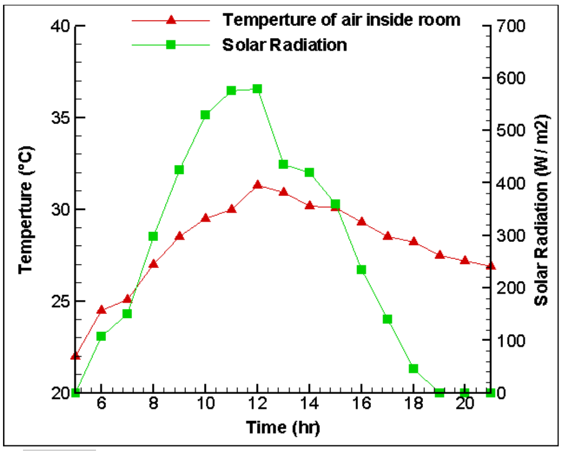

Fig. 7 Solar Radiation Intensity and the air temperature inside the test room Over Time on The Selected Day, 15 March 2023.

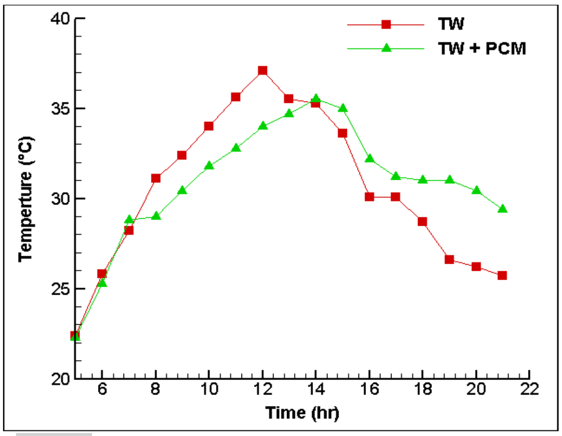

Fig. 8 Temperature variation of the internal surface of the Two Types Triple Glazed Window with Time on 15 March 2023.

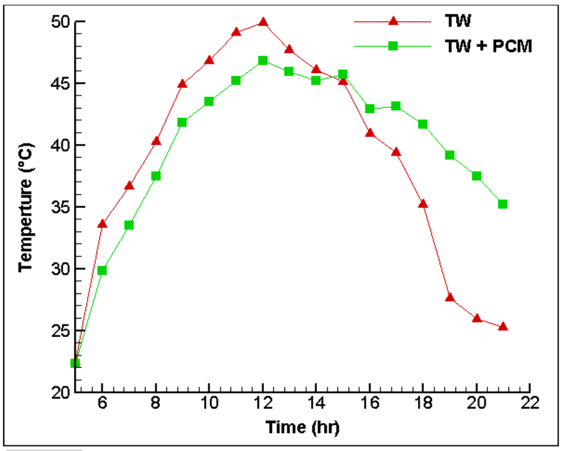

Fig. 9 Hourly external surface temperature of The TW and (TW With PCM) on 15 March 2023.

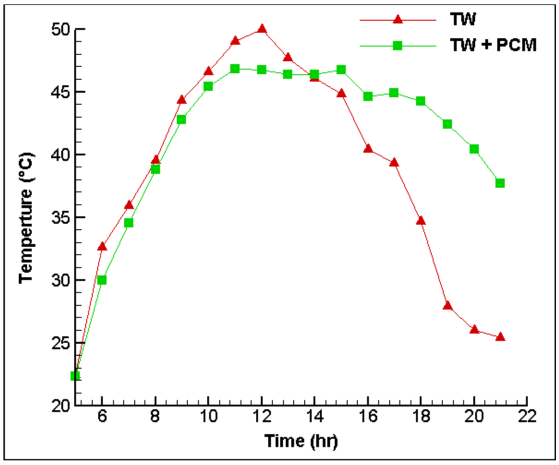

(a)

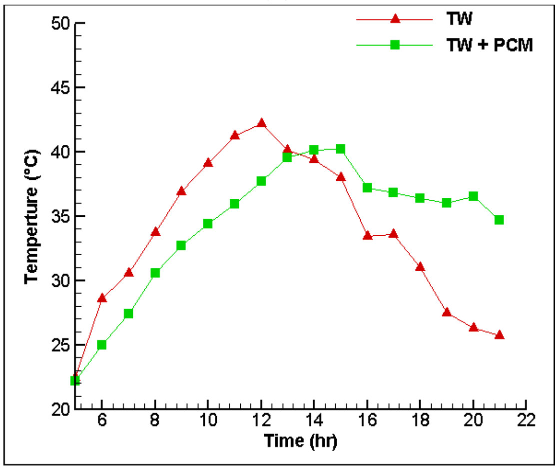

(b)

Fig. 10 Hourly Gap temperature of the TW and (TW with PCM) on 15 March 2023: (a) Outer Gap, (b) Inner Gap.

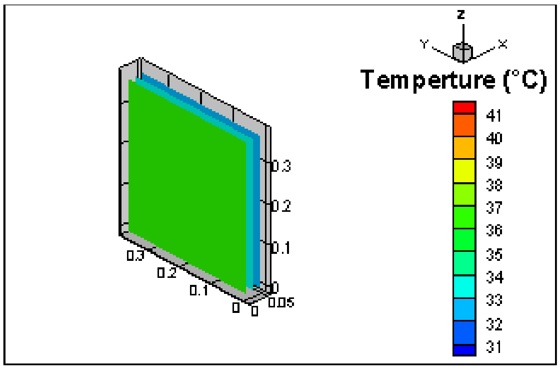

(a)

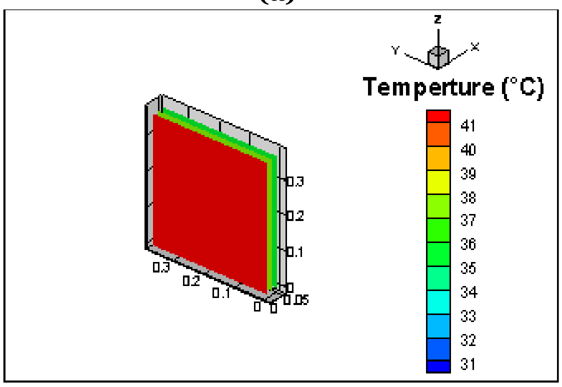

(b)

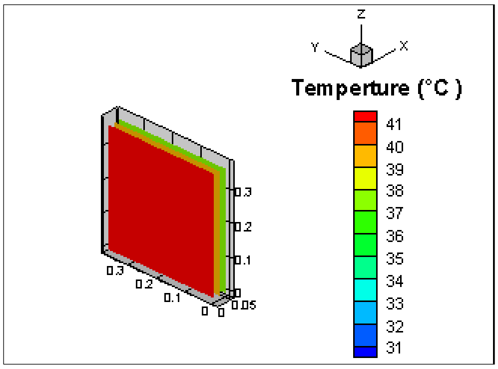

(c)

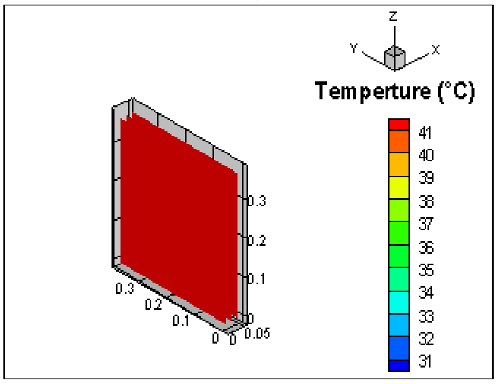

(d)

Fig. 11 Isothermal Contours of Triple Glazed Window with Phase Change Material (TW-PCM) In March at Various Times, (a) 9:00 AM, (b) 11:00 PM, (c) 12:00 PM, and (d) 4:00 PM.

4.2.Comparison with Previous Studies

Figure 12 compares the internal of the surface temperature in reference [26] with (TW and TW+PCM) in March data for the current investigation. The differentiation was conducted over the duration (15 h) from 6 AM to 9 PM. Under same conditions, i.e., relatively the same solar radiation. The TW two-configuration shows to be the best for minimizing peak internal temperatures due to using triple-glazed windows and PCM, delaying maximum time of the temperature compared to reference [26].

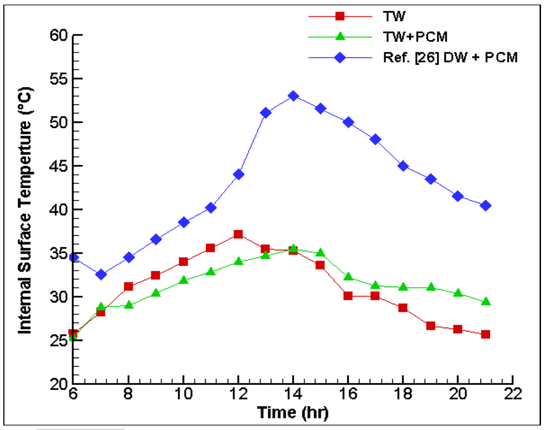

Fig. 12 Comparison of the Difference in Internal Surface Temperature between the TW and TW+PCM in the Present Work and Ref. [26].

5.CONCLUSION

The performance of thermal heat for TW was estimated under two separate configurations: without PCM and with PCM. This assessment aimed to determine the effects of these two windows. From the results, several conclusions were reached:

1) Integrating PCM as an insulating material led to a noticeable reduction in the inner surface temperature of the TW in March, when solar radiation peaked at 580 W/m2. The interior surface temperature of the TW embedded with PCM (TW-PCM) was 3.1 °C lower than the standard TW without PCM.
2) In the TW-PCM configuration, the thermal time lag was extended by approximately 2 hours, effectively delaying the peak thermal load.
3) The differentiation between the numerical and experimental results provides appreciable confirmation, suggesting that the proposed test model can accurately predict the phase change process and its impact on the test chamber.
4) The TW with phase change materials offered the best thermal performance under the same external conditions by utilizing the PCM's latent heat property, i.e., storing excess energy in abundance times and releasing it when it is required, thus achieving a moderate temperature and a comfortable environment for humans inside buildings and reducing the need for expensive heating and cooling devices.
5) The experimental and numerical results were highly agreeable, indicating that the suggested model can correctly estimate the phase-changing process and its effect on the room.

ACKNOWLEDGEMENTS

This work was conducted in the Mechanical Department of the National School of Engineers of Sfax (ENIS), in collaboration with the Advanced Fluid Dynamics Energy and Environment Laboratory (LDFAEE) and the Electromechanical Engineering Department at the University of Technology (UOT), under the supervision of Dr. Mounir Baccar, Professor at ENIS, and Dr. Jalal M. Jalil, Professor at UOT.

NOMENCLATURE

a_n+a_s+a_e+ a_w+a_t+a_b	Coefficients in general Finite-Volume equations
Cp	Specific heat of air, kJ/(kg. °C)
Cp_s	Specific heat of solid phase, kJ/(kg °C)
Cp_l	Specific heat of liquid phase, kJ/(kg °C)
dt	Time step, s
d_g	Glass density, kg/m^3
dx, dy, dz	Grid spacing
H	Enthalpy, kJ/kg
I	Intensity of solar radiation, W/m^2
i, j, k	indices which position in the (x, y, z) directions.
k	Thermal conductivity, W/ (m °C)
k_g	Glass thermal conductivity, W/(m. °C)
k_l	liquid thermal conductivity, W/ (m °C)
k_s	Solid thermal conductivity W/ m °C
l	Liquid
l_x, l_y, l_z	Distance of (x, y, z)
L	Latent heat, kJ/kg
N	North neighbor of grid P
P	Grid point
Q	Heat generation per unit volume W/m^3
$\bar{q}$	Average heat generation
S	South neighbor of grid P
T_s	Solid temperature of paraffin wax, °C
T_m	Melting temperature of paraffin wax, °C
T	Temperature °C)
T	Time, sec
T^*	Kirchhoff temperature °C
T	Top neighbor of grid P
dt	Time step, s
t	Control-volume face between P and T
V	Volume, m^3
W	West neighbor of grid P
W	Control-volume face between P and W
x, y, z	Cartesian coordinates (m)
Greek symbols	
ρ	Density, kg/m^3
λ	Diffusion coefficient
η	Dummy variable
∂	Partial derivative
Subscripts	
s	Solid
Abbreviations	
TW	Triple glazed window without PCM.
TW-PCM	Triple glazed window with PCM.
TTL	Temperature-Time Lag.
TDF	Temperature Decrement Factor
PCM	Phase change materials.
ESP-r	Environmental Systems Performance - Research
SAHs	Solar air heaters integrated with PCM.
SA-PCM	Silica aerogel and PCM
SSPCM	Solid-liquid PCM with solid-solid PCM.

REFERENCES

[1] Alnaieli HA, Jadallah AA, Numan HA. **Design, Fabrication, and Experimental Analysis of a PV Panel for a Smart Sunflower System**. *Tikrit Journal of Engineering Sciences* 2024; **31**(1): 113-126.

[2] Al-Sharo YM, Al Smadi K, Al Smadi K, Kamil NY. **Optimization of Stable Energy PV Systems Using the Internet of Things (IoT)**. *Tikrit Journal of Engineering Sciences* 2024; **31**(1): 127-137.

[3] Conti JP, Diefenderfer HJ, LaRose A, Turnure JT, Westfall L. DC (United States): USDOE Energy Information Administration (EIA), Office of Energy Analysis, *International Energy Outlook 2016 with Projections to 2040*. Washington, 2016.

[4] da Cunha JP, Eames P. **Thermal Energy Storage for Low and Medium Temperature Applications Using Phase Change Materials–a Review**. *Applied Energy* 2016; **177**: 227-238.

[5] Alam T, Dhau J, Goswami DY, Stefanakos E. **Microencapsulation and Characterization of Phase Change Materials for Latent Heat Thermal Energy Storage Systems**. *Applied Energy* 2015; **154**: 92–101.

[6] Memon ShA, Liao W, Yang Sh, Cui H, Shah SFA. **Development of Composite PCMs by Incorporation of Paraffin Into Various Building Materials**. *Materials* 2015; **8**: 499–518.

[7] Shi X, Memon SHA, Tang W, Cui H, Xing F. **Experimental Assessment of Position of Macro Encapsulated Phase Change Material in Concrete Walls on Indoor Temperatures and Humidity Levels**. *Energy and Buildings* 2014; **71**: 80–87.

[8] Xie N, Luo J, Li Z, Huang Z, Gao X, Fang Y, Zhang ZZ. **Salt Hydrate/Expanded Vermiculite Composite as a Form-Stable Phase Change Material for Building Energy Storage**. *Solar Energy Materials and Solar Cells* 2019; **189**: 33–42.

[9] Bao X, Tian Y, Yuan L, Cui H, Tang W, Fung WH, Qi H. **Development of High Performance PCM Cement Composites for Passive Solar Buildings**. *Energy and Buildings* 2019; **194**: 33–45.

[10] Abbas HM, Jalil JM, Ahmed ST. **Experimental and Numerical Investigation of PCM Capsules as Insulation Materials Inserted Into a Hollow Brick Wall**. *Energy and Buildings* 2021; **246**: 111127.

[11] Jalil JM, Mahdi HS, Allawy AS. **Cooling Performance Investigation of PCM Integrated into Heat Sink with Nano Particles Addition**. *Journal of Energy Storage* 2022; **55** (Part A): 105466.

[12] Wieprzkowicz A, Heim D. **Modelling of Thermal Processes in a Glazing Structure with Temperature Dependent Optical Properties - An Example of PCM-Window**. *Renewable Energy* 2020; **160**: 653-662.

[13] Dheyab HS, Al-Jethelah MSM, Ibrahim ThK, Chtourou S. **Closed Solar Air Heater System Integrated with PCM (RT42 and RT50) in a Thermal Storage-Finned Heat Exchanger Unit**. *Tikrit Journal of Engineering Sciences* 2023; **30**(3): 27-37.

[14] Ahmed OK, Hamada KI, Salih AM, Daoud RW. **A State of the Art Review of PV-Trombe Wall System: Design and Applications**. *Environmental Progress & Sustainable Energy* 2020; **39**(3): e13370, (1-40).

[15] Ahmed OK, Hamada KI, Salih AM. **Performance Analysis of PV/Trombe with Water and Air Heating System: An Experimental and Theoretical Study**. *Energy Sources, Part A: Recovery, Utilization, and Environmental Effects* 2019; **44**: 2535–2555.

[16] Abbas EF, Azat ShA. **The Impact of Width of the Air Gap Channel on the Mass Flow Rate, Rayleigh Number, and Efficiency of Passive Solar Heating System**. *Tikrit Journal of Engineering Sciences* 2018; **25**(3): 47-52.

[17] Salih SM, Jalil JM, Najim SE. **Experimental and Numerical Analysis of Double-Pass Solar Air Heater Utilizing Multiple Capsules PCM**. *Renewable Energy* 2019; **143**: 1053-1066.

[18] Zhang Ch, Yang R, Lu Y, Arıcı M, Ma Y, Yang X, Qi Z, Li D. **Parametric Research on Thermal and Optical Properties of Solid-Solid Phase Change Material Packaged in Glazing Windows**. *Journal of Energy Storage* 2024; **83**: 110562.

[19] Kułakowski T, Węglarz A, Heim D. **An Optimisation Study of PCM Triple Glazing for Temperate Climatic Conditions – Dynamic Analysis of Thermal Performance**. *Energy* 283 2023; **283**: 128361.

[20] Wang Sh, Zhang Ch, Zhang Sh, Zhou Y, Arıcı M. **Characteristics of PCMs-Filled Double Glazing Unit under Fire: A Detailed Thermal Structural Analysis**. *Journal of Building Engineering* 2023; **65**: 105672.

[21] Li D, Ma Y, Zhang Sh, Yang R, Zhang Ch, Liu Ch. **Photothermal and Energy Performance of an Innovative Roof Based on Silica Aerogel-PCM Glazing Systems**. *Energy Conversion and Management* 2022; **262**: 115567.

[22] Li D, Li Z, Zheng Y, Liu Ch, Hussein AK, Liu X. **Thermal Performance of a PCM Filled Double-Glazing Unit with Different Thermophysical Parameters of PCM**. *Solar Energy* 2016; **133**: 207–220.

[23] Sun G, Sh Li, Xu G, Zhang X. **Experimental Study on the Dynamic Heat Transfer Characteristics of Triple-Pane PCM-Filled Window**. *Sustainable Cities and Society 2016: Proceedings of the 12th REHVA World Congress*; Denmark. Aalborg University.

[24] Li Sh, Zhong K, Zhou Y, Zhang X. **Comparative Study on the Dynamic**

Heat Transfer Characteristics of PCM-Filled Glass Window and Hollow Glass Window. *Energy and Buildings* 2014; **85**: 483–492.

[25] Jalal MJ, Salih MS. **Analysis of Thermal and Insulation Performance of Double-Glazed Window Doped with Paraffin Wax**. *Engineering and Technology Journal* 2020; **38**: 383-393.

[26] Jalil JM, Salih SM. **Experimental and Numerical Investigation of Paraffin Wax as Thermal Insulator in a Double-Glazed Window**. *Journal of Energy Storage* 2021; **35**: 102173.

[27] Hasan MI, Basher HO, Shdhan AO. **Experimental Investigation of Phase Change Materials for Insulation of Residential Buildings**. *Sustainable Cities and Society* 2018; **36**:42-58.

[28] Wang X, Yang Y, Li X, Li Ch. **Modeling, Simulation, and Performance Analysis of a Liquid-Infill Tunable Window**. *Sustainability* 2022; **14**:15968.

[29] Nowzari R, Aldabbagh LBY, Egelioglu F. **Single and Double Pass Solar Air Heaters with Partially Perforated Cover and Packed Mesh**. *Energy* 73 2014; **73**: 694–702.

[30] Cao Y, Faghri A, Chang WS. **A numerical Analysis of Stefan Problems for Generalized Multidimensional Phase-Change Structures Using the Enthalpy Transforming Model**. *International Journal of Heat and Mass Transfer* 1989; **32**: 1289-1298.

[31] Jalil MJ, Abdulmunem, RA, Abed HA. **Numerical and Experimental Investigation of Using Inner Longitudinal Fins in a Rectangular Encapsulation on the PCM Melting Behaviors**. *Journal of Engineering and Sustainable Development* 2016; **20**: 139-154.

[32] Norton T, Delgado A, Hogan E, Grace P, Sun DW. **Simulation of High-Pressure Freezing Processes by Enthalpy Method**. *Journal of Food Engineering* 2009; **91**: 260–268.

[33] Cho SH, Sunderland JE. **Heat-Conduction Problems with Melting or Freezing**. *ASME Journal of Heat and Mass Transfer* 1969; **91**: 421-426.